Selective harmonic elimination technique with control of capacitive DC-link voltages in an asymmetric cascaded H-Bridge Inverter for STATCOM Application

Sajadi, Rahman; Iman-Eini, Hossein; Bakhshizadeh, Mohammad Kazem; Neyshabouri, Yousef; Farhangi, Shahrokh

Published in:
IEEE Transactions on Industrial Electronics

DOI (link to publication from Publisher):
10.1109/TIE.2018.2811365

Publication date:
2018

Document Version
Accepted author manuscript, peer reviewed version

Selective Harmonic Elimination Technique with Control of Capacitive DC Link Voltages in an Asymmetric Cascaded H-Bridge Inverter for STATCOM Application

Rahman Sajadi, Hossein Iman-Eini, *Senior Member, IEEE*, Mohammad Kazem Bakhshizadeh, *Student Member, IEEE*, Yousef Neyshabouri and Shahrokh Farhangi, *Member, IEEE*

***Abstract*—In this paper, selective harmonic elimination (SHE) technique is introduced for a cascaded H-Bridge based STATCOM (CHB-STATCOM) with unequal capacitive dc-link voltages. The asymmetric topology allows increasing the number of voltage levels while keeping the converter losses low. Moreover, reactive power control is realized by using the decoupled current control and the voltage of individual capacitors is controlled by the help of SHE modulation. Mathematical equations are derived for synthesizing the multilevel ac waveform and regulation of dc-link voltages for a CHB inverter with an arbitrary number of H-bridge cells. Then, to verify the theoretical claims, simulation and experimental results are provided for a three-phase CHB inverter with two H-bridge cells in each phase.**

***Index Terms*— asymmetric dc-links, Cascaded H-bridge (CHB), selective harmonic elimination modulation (SHE), STATCOM.**

I. Introduction

FACTS devices are commonly used to improve the power quality in power systems. Static VAR compensator (STATCOM) is one of these devices which has caught more attention in the last decade. For implementation of STATCOM, multilevel converters can be utilized due to their interesting merits such as lower harmonic generation and better efficiency than conventional two level converters [1]. The three most popular types of multilevel converter are categorized as 1) flying capacitor 2) diode clamped and 3) cascaded H-bridge (CHB) converter [2]-[8]. Due to the modularity and having a lower number of components for synthesizing the same number of voltage levels, the CHB structure is a better choice for STATCOM applications.

Traditionally, to obtain low harmonic distortion in the output voltage waveform of a symmetric CHB, the number of modules or the switching frequency are increased which leads to higher cost or power losses, respectively. Asymmetric cascaded H-bridge inverter is an alternative approach to avoid these problems [9]. In this topology, by selecting unequal voltage values for the dc-link capacitors, the number of voltage levels is increased and consequently the quality of output waveform is improved. Furthermore, in this topology, the switching frequency of H-bridge cells has a reverse relation to the dc-link voltages. In other words, the cells with higher voltages will have lower switching frequencies, which leads to lower power losses and better efficiency. The advantages of the asymmetric multilevel CHB inverter has been investigated in [10], [11] for the drive application. Both the symmetric and asymmetric CHB structures need isolated dc sources which can be cumbersome; but, in reactive power compensation applications, this issue can be overcome by utilizing capacitive dc-links instead of isolated dc voltage sources [12]. Hence, the control system of the CHB based STATCOM should fulfil the following objectives: 1) reactive power control in the network and 2) regulation of capacitors' voltages. Several solutions for regulation of capacitors' voltages in CHB-STATCOM have been proposed in literature. In [12]-[17], the dc-link voltage balancing has been achieved by inserting a compensation term to the modulation voltage of H-bridge cells in the phase shift pulse width modulation (PS-PWM). In these methods, voltages of capacitors are regulated to a fixed value which makes them inapplicable for asymmetric inverters. Refs. [18]-[20] employ switching redundancies to produce different voltage levels and to regulate the capacitors voltages to unequal values.

Two methods are introduced in [9] and [21] to maintain the capacitors' voltages in predetermined values in an asymmetric CHB-STATCOM. These strategies are based on hybrid modulation technique, where the cell with higher voltage is switched in low frequency and the cell with low voltage is switched in high frequency. In these methods, for each H-bridge cell, an individual voltage control loop is needed which makes the whole control system more complex.

Selective harmonic elimination (SHE) has been suggested in [22] as a modulation technique for a CHB based STATCOM. In SHE technique, the low switching frequency is employed and the converter losses is the minimum possible value. In [22], instead of capacitive dc-links, dc power sources

Manuscript received Aug 21, 2017; revised Nov 15, 2017; accepted Feb 13, 2018. This work was supported by the Iran National Science Foundation (INSF).

R. Sajadi, H. Iman-Eini, Y. Neyshabouri and Sh. Farhangi are with the School of Electrical and Computer Engineering, College of Engineering, University of Tehran, Tehran, Iran (e-mail: rahman.sajadi@ut.ac.ir; imaneini@ut.ac.ir; y.neyshabouri@ut.ac.ir; farhangi@ut.ac.ir).

M. K. Bakhshizadeh, is with the Department of Energy Technology, Aalborg university, Aalborg, Denmark (e-mail: mok@et.aau.dk).

This article has been accepted for publication in a future issue of this journal, but has not been fully edited. Content may change prior to final publication. Citation information: DOI 10.1109/TIE.2018.2811365, IEEE Transactions on Industrial Electronics

with Buck converters have been employed to generate asymmetric dc voltages. Necessity to Buck converters will increase the number of components and the system complexity which are not desirable for high power applications.

In this paper, a novel SHE modulation technique is introduced for implementation of asymmetrical CHB based STATCOM with capacitive dc-links. In this method, the SHE modulation equations are derived to eliminate low order harmonics and also to regulate the voltage of dc-link capacitors to desired values.

The structure of this paper is organized as follows: section II describes the CHB based STATCOM. The proposed control system for voltage regulation is presented in section III and IV. To verify the proposed control system, simulation and experimental results are provided in section V and VI. Conclusions are given in section VII.

II. CONFIGURATION OF CHB BASED STATCOM

Fig .1 shows the structure of a three-phase CHB-based STATCOM, where L*s* is the filter inductance, R*s* is the equivalent resistance of the filter, and $V_{s,abc}$ and $V_{c,abc}$ are three-phase voltages of the network and the output voltage of CHB inverter, respectively. The structure of each cell that contains four switches with anti-parallel diodes and one dc-link capacitor is depicted in Fig. 2. For modeling the switching and conduction losses in each cell, a parallel resistor (R_{dc}) is added to the dc-link of each cell [12], [23].

From Fig. 1, the equations of CHB based STATCOM can be written as follows:

$$L_s \frac{di_a}{dt} + R_s i_a = V_{sa} - V_{ca} \quad (1)$$

$$L_s \frac{di_b}{dt} + R_s i_b = V_{sb} - V_{cb} \quad (2)$$

$$L_s \frac{di_c}{dt} + R_s i_c = V_{sc} - V_{cc} \quad (3)$$

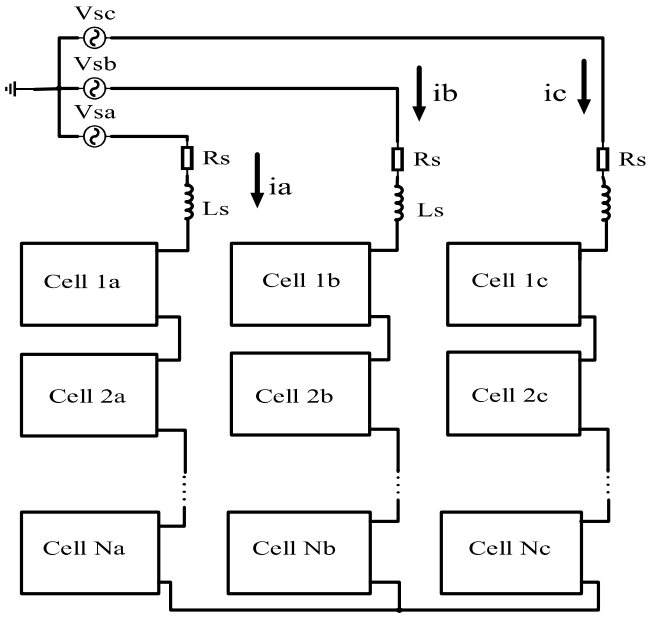

Fig. 1. Block diagram of CHB based STATCOM.

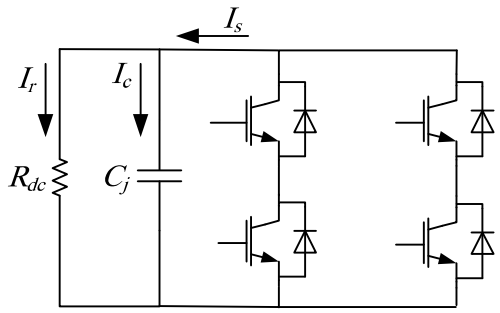

Fig. 2. Block diagram of one arbitrary H-bridge cell in Fig.1

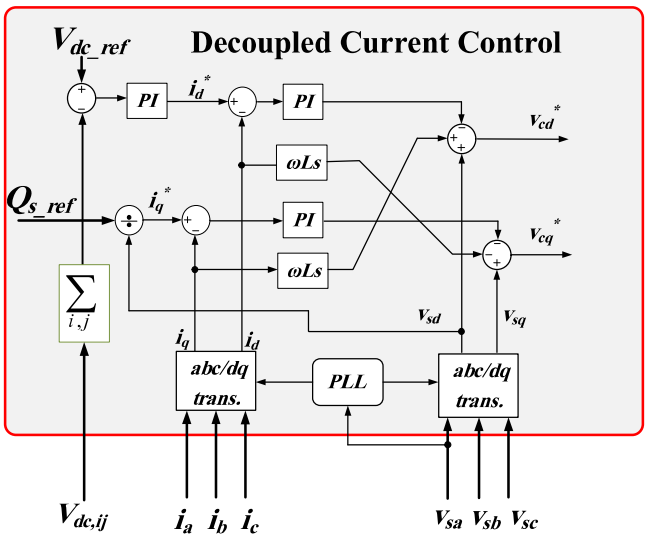

Fig. 3. Employed decoupled current control for STATCOM.

Many solutions have been proposed to control this system. One of these methods is known as decoupled active and reactive power control. Section III describes this control approach in details [3]-[4], [7], [12]-[14].

III. DECOUPLED CURRENT CONTROL

In this control method, the system equations (1)-(3) in abc stationary frame are transformed into d-q synchronous frame and the equations can be written as:

$$L_s \frac{d}{dt}\begin{bmatrix} i_d \\ i_q \end{bmatrix} + R_s \begin{bmatrix} i_d \\ i_q \end{bmatrix} + \begin{bmatrix} 0 & -\omega L_s \\ \omega L_s & 0 \end{bmatrix} \begin{bmatrix} i_d \\ i_q \end{bmatrix} = \begin{bmatrix} V_{sd} - V_{cd} \\ V_{sq} - V_{cq} \end{bmatrix} \quad (4)$$

where i_d and i_q represent the d axis and q axis current terms, V_{sd},V_{sq} represent the d axis and q axis voltage terms of grid voltage and V_{cd}, V_{cq} are the d axis and q axis components of the inverter voltage. Also, $\omega = \frac{d\alpha}{dt}$ is the angular frequency and α represents the phase of system voltage. Then, the active and reactive power flow in CHB based STATCOM can be defined by:

$$P = -V_{sd} i_d - V_{sq} i_q \quad (5)$$

$$Q = V_{sd} i_q - V_{sq} i_d \quad (6)$$

If the d axis of dq reference frame is aligned to V_{sa}, the value of V_{sq} will be zero and the active and reactive powers

This article has been accepted for publication in a future issue of this journal, but has not been fully edited. Content may change prior to final publication. Citation information: DOI 10.1109/TIE.2018.2811365, IEEE Transactions on Industrial Electronics

can be controlled independently. Now, one can define the d-axis and q-axis reference currents by (7) and (8), respectively.

$$i_d^* = \frac{P^*}{V_{sd}} \tag{7}$$

$$i_q^* = \frac{Q^*}{V_{sd}} \tag{8}$$

In above equations, active power reference is determined from the output of a PI regulator utilized for regulation of average dc-link voltages, and the reactive power reference is set by the higher level control system. The sum of dc-link voltage cells is calculating by:

$$V_{dc-sum} = \sum_{i=a,b,c} \sum_{j=1}^{N} V_{dcij} \tag{9}$$

where V_{dcij} is the voltage of j^{th} H-bridge cell in the i^{th} phase. With equations (4)-(9), the block diagram of control system can be obtained and shown as Fig. 3.

According to Fig. 3, reference voltages of the inverter V_{cd}^* and V_{cq}^* can be obtained and applied by a proper modulation technique to the inverter. From these two reference values, the modulation index (M) and the phase difference between the inverter voltage and the grid voltage (δ), for controlling the active and reactive power, can be determined as:

$$M = \frac{\sqrt{(V_{cd}^*)^2 + (V_{cq}^*)^2}}{NV_{dc\_ref}} \tag{10}$$

$$\delta = a\tan\left(\frac{V_{cq}^*}{V_{cd}^*}\right) \tag{11}$$

If the CHB inverter can synthesize the ac terminal voltages according to (10) and (11), the control goals including the reactive power control and regulation of average voltage of all dc-links will be satisfied. However, for achieving desired voltage values (or unequal values) for individual dc-links, a supplementary control system is required. This control method is described in the next section.

TABLE I
COMPARISON OF SYMMETRIC AND ASYMMETRIC CHBS

DC link voltage ratio	Number of redundant states	Number of voltage levels
1:1:1…:1	3^N-2N-1	2N+1
1:2:4…2^{N-1}	3^N-2^{N+1}+1	2^{N+1}-1
1:3:9…3^{N-1}	0	3^N

IV. VOLTAGE REGULATION OF INDIVIDUAL DC LINKS

Voltage regulation of individual dc-links is achieved by the SHE modulation. In other words, this modulation technique is utilized not only for reduction of switching losses, but also for regulation of individual dc-links. In this modulation technique, at first, the appropriate switching instants for controlling the fundamental harmonic, elimination of low order harmonics, and regulation of dc-link voltages are determined by off-line calculations; then, switching angles are stored in look-up tables to be used by the inverter control system.

As mentioned earlier, the hybrid (or asymmetric) multilevel inverter generates higher number of voltage levels in its output, which makes it a desired choice for power quality applications. In Table I, different dc voltage ratios for a CHB inverter with N cells in each phase is considered and the corresponding number of redundant switching states and the total number of voltage levels which can be synthesized are given. For example, first row shows the symmetric case where the voltages of dc links are equal together. Second and third rows are related to asymmetric cases where the voltage of dc links are set as (V_{dc}, $2V_{dc}$, .., $2^{N-1}V_{dc}$) or (V_{dc}, $3V_{dc}$, .., $3^{N-1}V_{dc}$), respectively. The readers are referred to [24] for further explanations.

In this paper, the dc voltage ratio (1:3:9…) is chosen to synthesize the highest number of voltage levels, according to Table I. Fig. 4 shows a predefined switching pattern for a converter with N cells in each phase with dc-link ratio of (1:3:9..) and 3^N voltage levels at the ac terminal. In the following, the mathematical calculations for finding the switching angles are given, where dc-link voltages are regulated by the modulation technique. By applying the

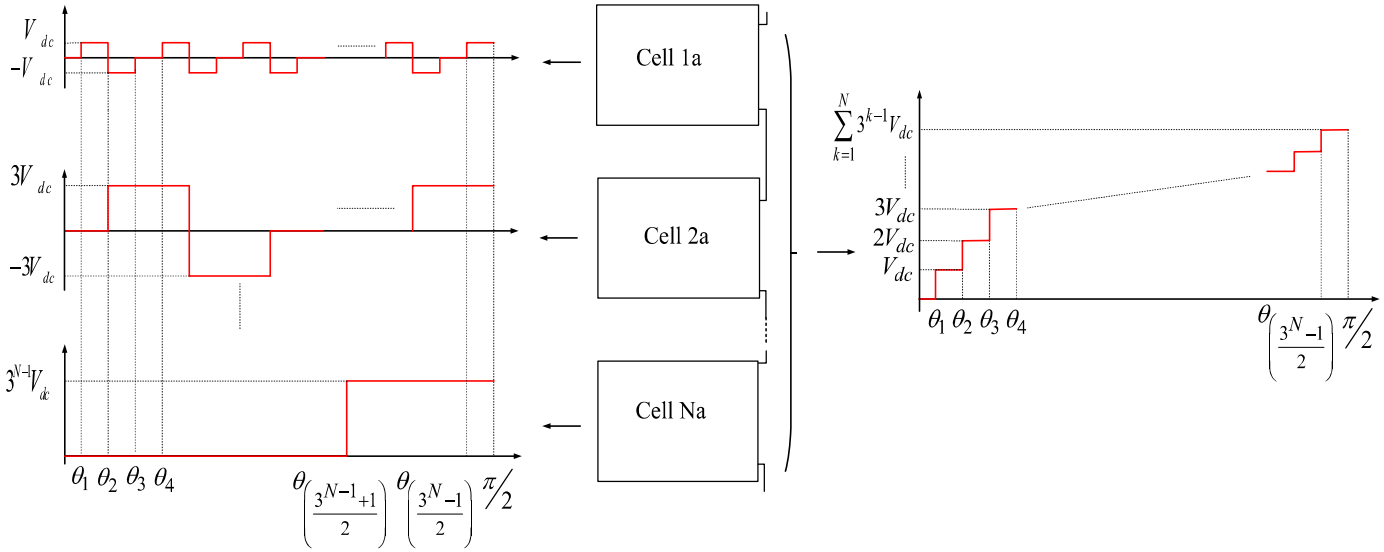

Fig. 4. Mechanism of voltage generation in each cell of phase-a (left side) and total ac terminal voltage (right side).

Fourier analysis to the predefined waveform in Fig. 4, the following relations are derived for the fundamental, 5th , 7th … harmonic terms:

$$\begin{aligned} V_f &= \frac{4}{\pi}\int_0^{\pi/2} V\sin(\omega t)\,d\omega t \\ &= \frac{4V_{dc}}{\pi}\left(\cos\theta_1+\cos\theta_2+\ldots+\cos\theta_{\left(\frac{3^N-1}{2}\right)}\right) \\ &\left(\cos n\theta_1+\cos n\theta_2+\ldots+\cos n\theta_{\left(\frac{3^N-1}{2}\right)}\right)=0 \ , \quad n=5,7,\ldots \end{aligned} \tag{12}$$

where V_f is the amplitude of fundamental harmonic, θ_1, θ_2, … are switching angles and n represents the harmonic order. Fig. 2 shows the capacitor current for an arbitrary cell which is written by:

$$\begin{cases} I_c = I_s - I_r \\ I_s = I_m\sin(\omega t+\varphi) \\ I_r = \dfrac{V_{dcj}}{R_{dc}} \end{cases} \tag{13}$$

where φ represents the phase angle between the grid voltage and grid current and I_m is the amplitude of grid current. One can obtain the charging equation for the jth capacitor by (14):

$$Q_j = \int\left(I_m\sin(\omega t+\varphi)-\frac{V_{dcj}}{R_{dc}}\right)dt \tag{14}$$

Using (14) and noting to the waveform in Fig. 4, the charging equation for any of capacitors in one period is obtained as (15). By doing some more calculations, (15) can be simplified as (16).

$$\begin{aligned} Q_j &= \int_0^{2\pi}\left(I_m\sin(\omega t+\varphi)-\frac{V_{dcj}}{R_{dc}}\right)dt = \int_{\theta_{\left(\frac{3^{j-1}+1}{2}\right)}}^{\theta_{\left(\frac{3^j+1}{2}\right)}} I_m\sin(\omega t+\varphi)\,d\omega t + \int_{\theta_{\left(\frac{3^j+1}{2}\right)}}^{\theta_{\left(\frac{3^{j+1}+1}{2}\right)}} -I_m\sin(\omega t+\varphi)\,d\omega t + \ldots \\ &+\int_{\theta_{\left(\frac{3^N-2*3^{j-1}+1}{2}\right)}}^{\pi/2} I_m\sin(\omega t+\varphi)\,d\omega t + \int_{\pi/2}^{\pi-\theta_{\left(\frac{3^N-2*3^{j-1}+1}{2}\right)}} I_m\sin(\omega t+\varphi)\,d\omega t + \ldots + \int_{\pi-\theta_{\left(\frac{3^j+1}{2}\right)}}^{\pi-\theta_{\left(\frac{3^{j-1}+1}{2}\right)}} I_m\sin(\omega t+\varphi)\,d\omega t \\ &+\int_{\pi+\theta_{\left(\frac{3^{j-1}+1}{2}\right)}}^{\pi+\theta_{\left(\frac{3^j+1}{2}\right)}} -I_m\sin(\omega t+\varphi)\,d\omega t + \int_{\pi+\theta_{\left(\frac{3^j+1}{2}\right)}}^{\pi+\theta_{\left(\frac{3^{j+1}+1}{2}\right)}} I_m\sin(\omega t+\varphi)\,d\omega t + \ldots + \int_{\pi+\theta_{\left(\frac{3^N-2*3^{j-1}+1}{2}\right)}}^{3\pi/2} -I_m\sin(\omega t+\varphi)\,d\omega t \\ &+\int_{3\pi/2}^{2\pi-\theta_{\left(\frac{3^N-2*3^{j-1}+1}{2}\right)}} -I_m\sin(\omega t+\varphi)\,d\omega t + \ldots + \int_{2\pi-\theta_{\left(\frac{3^j+1}{2}\right)}}^{2\pi-\theta_{\left(\frac{3^{j-1}+1}{2}\right)}} -I_m\sin(\omega t+\varphi)\,d\omega t - \int_0^{2\pi}\frac{V_{dcj}}{R_{dc}}dt \end{aligned} \tag{15}$$

$$Q_j = 4I_m\cos\varphi\left\{\begin{aligned} &\sum_{k=1}^{k=\left\lfloor\frac{3^N+5*3^{j-1}-2}{2*3^j}\right\rfloor}\left(\cos\theta_{3^{j-1}\left(3k-\frac{5}{2}\right)+\frac{1}{2}}\right)+\sum_{k=1}^{k=\left\lfloor\frac{3^N+3^j-2}{2*3^j}\right\rfloor}\left(-2\cos\theta_{3^{j-1}\left(3k-\frac{3}{2}\right)+\frac{1}{2}}\right) \\ &+\sum_{k=1}^{k=\left\lfloor\frac{3^N+3^{j-1}-2}{2*3^j}\right\rfloor}\left(\cos\theta_{3^{j-1}\left(3k-\frac{1}{2}\right)+\frac{1}{2}}\right) \end{aligned}\right\} \tag{16}$$

$$P_{in} = \frac{1}{2}V_f I_m\cos\varphi = \frac{\sum_{i=1}^{i=N}\left(3^{(i-1)}V_{dc}\right)^2}{R_{dc}} \Rightarrow I_m\cos\varphi = \frac{2*\sum_{i=1}^{i=N}\left(3^{(i-1)}V_{dc}\right)^2}{V_f R_{dc}} \tag{17}$$

$$\frac{V_{dc_j}}{V_{dc_i}} = \frac{\sum_{k=1}^{k=\left\lfloor\frac{3^N+5*3^{j-1}-2}{2*3^j}\right\rfloor}\left(\cos\theta_{3^{j-1}\left(3k-\frac{5}{2}\right)+\frac{1}{2}}\right)+\sum_{k=1}^{k=\left\lfloor\frac{3^N+3^j-2}{2*3^j}\right\rfloor}\left(-2\cos\theta_{3^{j-1}\left(3k-\frac{3}{2}\right)+\frac{1}{2}}\right)+\sum_{k=1}^{k=\left\lfloor\frac{3^N+3^{j-1}-2}{2*3^j}\right\rfloor}\left(\cos\theta_{3^{j-1}\left(3k-\frac{1}{2}\right)+\frac{1}{2}}\right)}{\sum_{k=1}^{k=\left\lfloor\frac{3^N+5*3^{i-1}-2}{2*3^i}\right\rfloor}\left(\cos\theta_{3^{i-1}\left(3k-\frac{5}{2}\right)+\frac{1}{2}}\right)+\sum_{k=1}^{k=\left\lfloor\frac{3^N+3^i-2}{2*3^i}\right\rfloor}\left(-2\cos\theta_{3^{i-1}\left(3k-\frac{3}{2}\right)+\frac{1}{2}}\right)+\sum_{k=1}^{k=\left\lfloor\frac{3^N+3^{i-1}-2}{2*3^i}\right\rfloor}\left(\cos\theta_{3^{i-1}\left(3k-\frac{1}{2}\right)+\frac{1}{2}}\right)} \tag{18}$$

This article has been accepted for publication in a future issue of this journal, but has not been fully edited. Content may change prior to final publication. Citation information: DOI 10.1109/TIE.2018.2811365, IEEE Transactions on Industrial Electronics

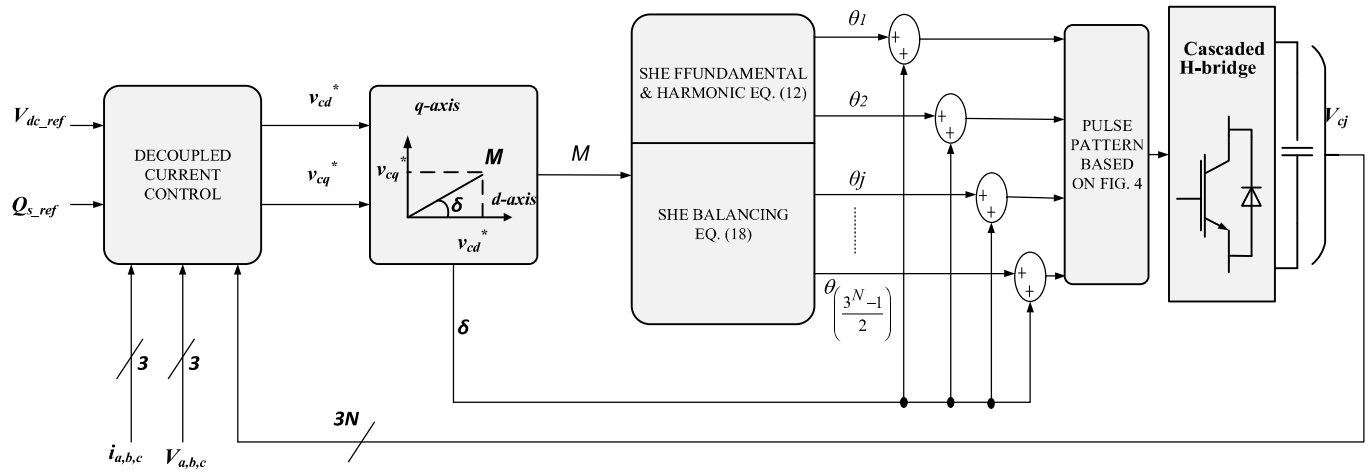

Fig. 5. Overall control in STATCOM for reactive power control and regulation of dc-link voltages at 1:3:9: voltage ratio.

Moreover, in steady state condition, the input active power to the converter is equal to cells losses, which is given in (17). Furthermore, the mean value of each capacitor voltage should remain constant at steady state; hence, the charge values in (16) are set to zero. Now by considering this point and combining (16), (17) and inserting V_f value from (12), (18) is obtained. Therefore, to guarantee the voltage regulation of capacitors, (18) must be satisfied in the corresponding SHE technique. In other words, by inserting the defined criterion in (18) to the SHE equations and solving the equations based on it, one can guarantee the voltage regulation of capacitors at the desired values, i.e., $V_{dc}, 3V_{dc}, \ldots, 3^{N-1}V_{dc}$.

It is worth noting that in the proposed set of SHE equations, there are $\left(\frac{3^N-1}{2}\right)$ degrees of freedom which are used to 1) control the amplitude of fundamental harmonic, 2) to eliminate the harmonic terms such as 5^{th}, 7^{th},…, and 3) to satisfy (18) by the remaining *N-1* degrees of freedom.

Fig. 5 illustrates the overall block diagram of control strategy. As it can be seen in Fig. 5, the decoupled current control system reads the capacitors' voltages, phase currents and grid voltages. Then based on differences between the estimated active and reactive powers and the active and reactive power references, the modulation index (*M*) and the phase shift (δ) are calculated. Finally, based on calculated *M, δ* and (12) and (18), the switching angles are computed and applied to the CHB inverter.

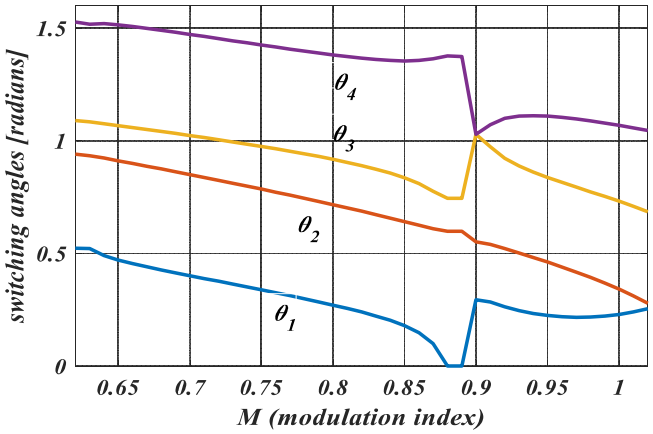

Fig. 6. Obtained Switching angles at different modulation indices.

In this method, by using the low frequency switching, switching losses are decreased and the efficiency is increased. By using asymmetric voltages in dc sides, the output waveform of inverter is enhanced compared to symmetric inverters. Also the capacitors' voltages are kept constant when the reference of reactive power is changed.

V. Simulation Results

To verify the proposed control method, several simulations have been done in PSCAD/EMTDC environment. Since the hardware prototype has *N*=2 cells in each phase, the simulations are also performed with the same number of H-

$$\frac{V_{dc_1}=3^{(1-1)}V_{dc}}{V_{dc_2}=3^{(2-1)}V_{dc}}=\frac{\sum_{k=1}^{k=\left\lfloor\frac{3^2+5*3^{1-1}-2}{2*3^1}\right\rfloor}\left(\cos\theta_{3^{1-1}\left(3k-\frac{5}{2}\right)+\frac{1}{2}}\right)+\sum_{k=1}^{k=\left\lfloor\frac{3^2+3^1-2}{2*3^1}\right\rfloor}\left(-2\cos\theta_{3^{1-1}\left(3k-\frac{3}{2}\right)+\frac{1}{2}}\right)+\sum_{k=1}^{k=\left\lfloor\frac{3^2+3^{1-1}-2}{2*3^1}\right\rfloor}\left(\cos\theta_{3^{1-1}\left(3k-\frac{1}{2}\right)+\frac{1}{2}}\right)}{\sum_{k=1}^{k=\left\lfloor\frac{3^2+5*3^{2-1}-2}{2*3^2}\right\rfloor}\left(\cos\theta_{3^{2-1}\left(3k-\frac{5}{2}\right)+\frac{1}{2}}\right)+\sum_{k=1}^{k=\left\lfloor\frac{3^2+3^2-2}{2*3^2}\right\rfloor}\left(-2\cos\theta_{3^{2-1}\left(3k-\frac{3}{2}\right)+\frac{1}{2}}\right)+\sum_{k=1}^{k=\left\lfloor\frac{3^2+3^{2-1}-2}{2*3^2}\right\rfloor}\left(\cos\theta_{3^{2-1}\left(3k-\frac{1}{2}\right)+\frac{1}{2}}\right)} \quad (19)$$

$$\rightarrow \frac{V_{dc}}{3V_{dc}}=\frac{\cos\theta_1-2\cos\theta_2+\cos\theta_3+\cos\theta_4}{\cos\theta_2} \quad (20)$$

This article has been accepted for publication in a future issue of this journal, but has not been fully edited. Content may change prior to final publication. Citation information: DOI 10.1109/TIE.2018.2811365, IEEE Transactions on Industrial Electronics

bridge cells. Hence, for the case of N=2 and according to Fig. 4 and (18), four degrees of freedom are obtained. One degree is used to control the fundamental harmonic, two degrees are dedicated to eliminate the 5th and 7th harmonic terms and the last one is used to regulate the capacitor voltages according to (20). In fact, by setting the parameters as: j=1, i=2 and N=2 in (18) and noting that V_{dci} and V_{dcj} are dc link voltages of i^{th} and j^{th} cell ($V_{dci} = 3^{(i-1)}V_{dc}$, $V_{dcj} = 3^{(j-1)}V_{dc}$), one can derive the following condition for voltage regulation.
Based on (18), one can derive (19) and then simplify it as (20) for N=2 cells.

Different methods have been presented in literature to solve the SHE equations. In this paper, Particle Swarm Optimization (PSO) method [25] is used and obtained switching angles at different modulation indices are illustrated in Fig. 6.

Table II shows the parameters of selected system for the simulation study. Also, Fig. 7 shows the phasor diagram of CHB-STATCOM in inductive and capacitive modes. in Fig. 7, the term V_s represents the amplitude of grid phase voltage, V_c is the output voltage of inverter which is equal to MV_f, M is the modulation index and V_f represents the fundamental harmonic of the output voltage of inverter which is determined by (12). In addition, R_s and L_s are the equivalent resistance and inductance of the network and I_s is the grid current. According to Fig. 7, in the capacitive mode (or when the reactive power is injected to the grid by STATCOM), V_c is greater than V_s. So in this condition, the modulation index will increase. On the other hand, in inductive mode (or when the reactive power is absorbed by the STATCOM), V_c is smaller than V_s. So in this condition, the modulation index will decrease [26]. Hence, from the design point of view, the maximum modulation index, i.e., M=1 is considered for full capacitive compensation mode and the minimum modulation index, i.e., M=0.6 is considered for full inductive compensation mode. It is worth

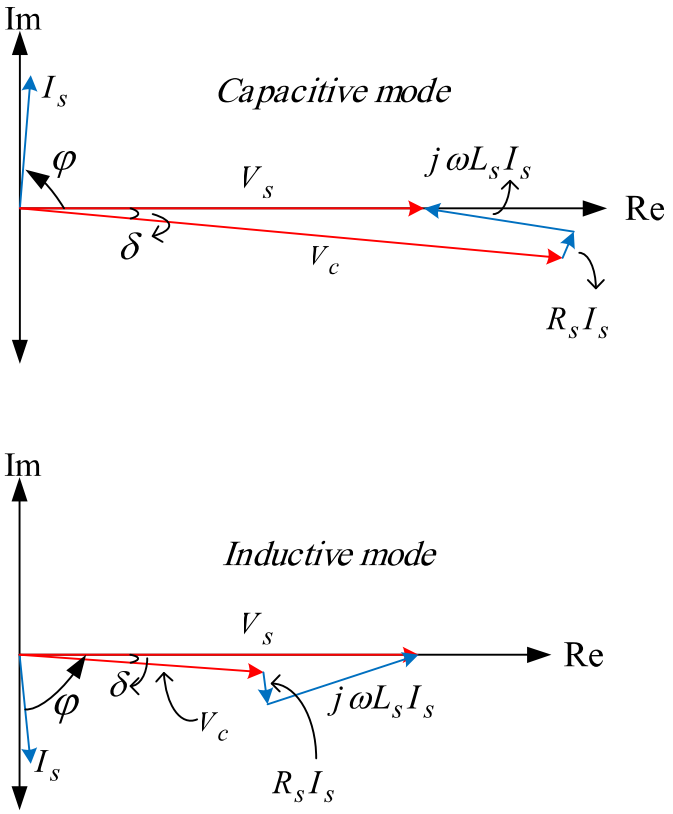

Fig. 7. Phasor diagram of CHB-STATCOM in capacitive and inductive modes.

TABLE II
PARAMETERS OF SIMULATION

Parameters	Value
Line-to-line voltage (V_s)	3.3 kV
Grid frequency (f_s)	50 Hz
Inductance of filter (L_s)	30 mH
DC link capacitance (C_{dc})	3.6 mF
Resistance of filter (R_s)	0.1 Ω
Higher power cell voltage ($3V_{dc}$)	2550 V
Lower power cell voltage (V_{dc})	850 V

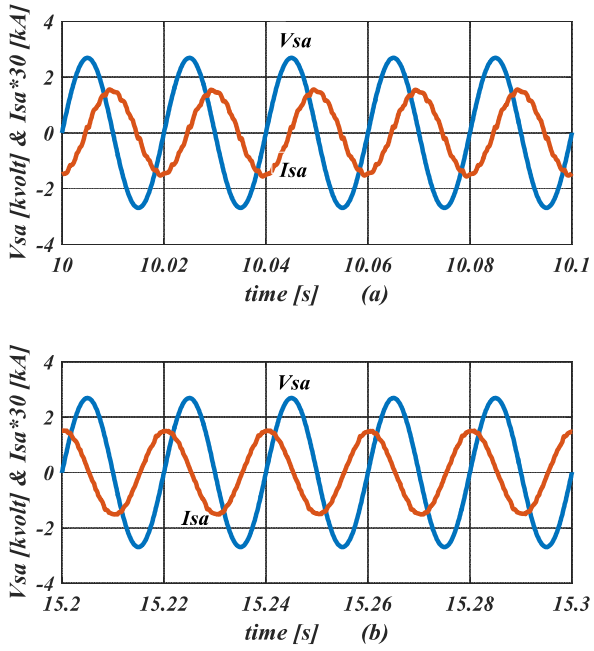

Fig. 8. Steady operation of STATCOM in a) inductive mode and b) capacitive mode.

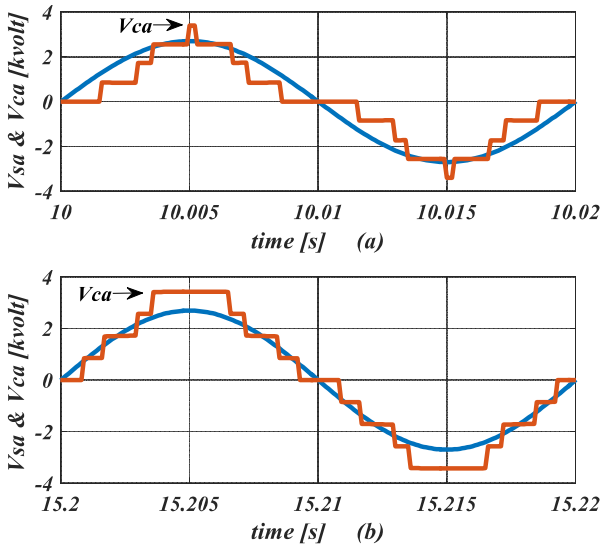

Fig. 9. Steady operation of STATCOM in a) inductive mode and b) capacitive mode.

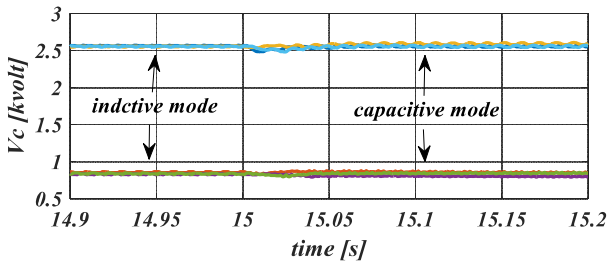

Fig. 10. Capacitor voltages in inductive and capacitive modes.

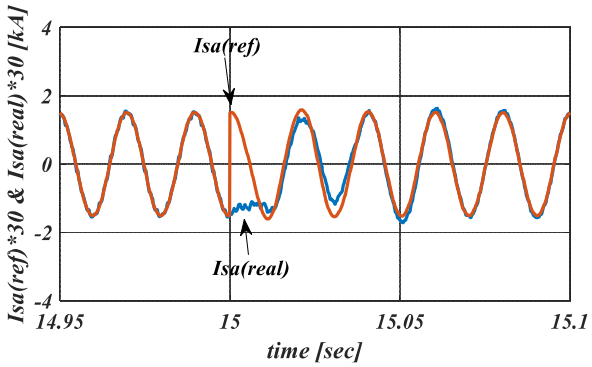

Fig. 11. Dynamic behavior of CHB inverter under step change of reactive power from -202kVAr to 202kVAr.

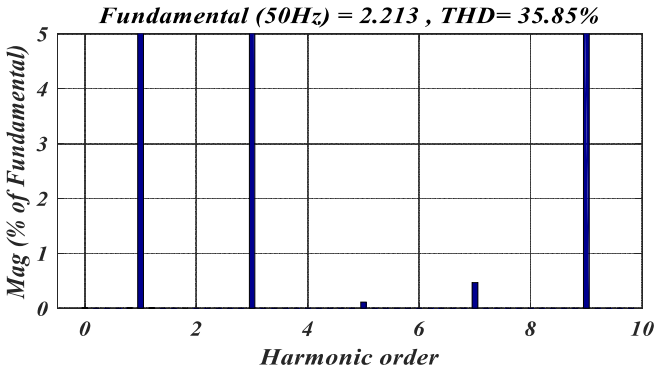

Fig. 12. Harmonic spectrum of output voltage.

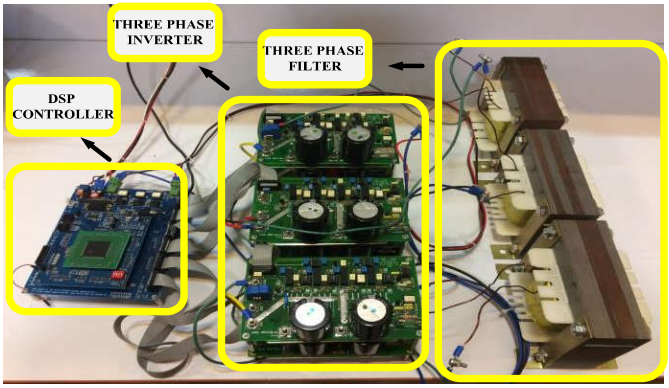

Fig. 13. Three phase CHB-STATCOM in laboratory structure.

mentioning that other operation points of the STATCOM, such as half capacitive and half inductive modes are located within the above range. In Fig. 6, it can be seen that by extracting the switching angles for the above modulation range, the whole reactive compensation range of the converter is covered. The simulation and experimental results of the full-capacitive and inductive modes are demonstrated in Figs 8, 9, 10 and 11 to confirm the feasibility and effectiveness of the proposed method.

TABLE III
PARAMETERS OF EXPERIMENTAL SETUP

Parameters	Value
Line-to-line voltage (V_s)	110 V
Grid frequency (f_s)	50 Hz
Inductance of filter (L_s)	8 mH
DC link capacitance (C_{dc})	3.6 mF
Resistance of filter (R_s)	0.1 Ω
Higher power cell voltage ($3V_{dc}$)	75 V
Lower power cell voltage (V_{dc})	25 V

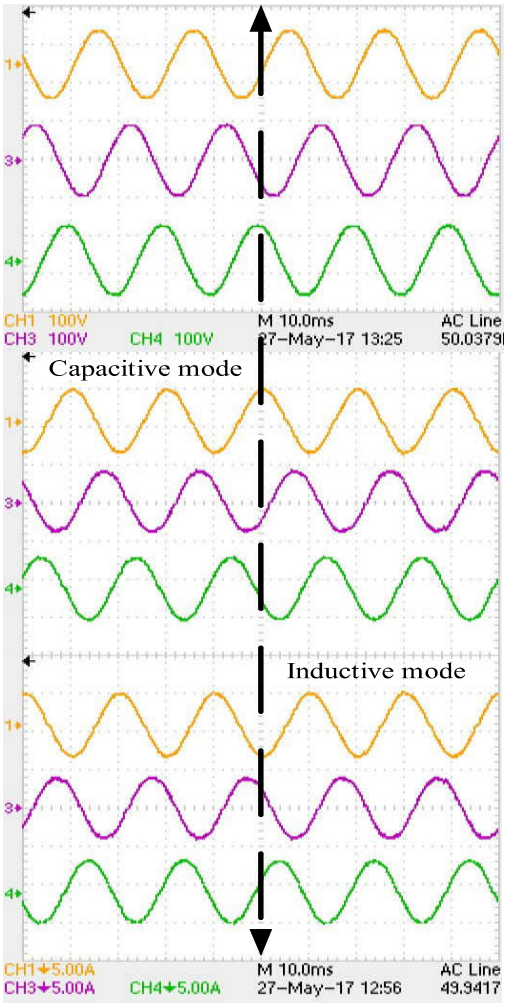

Fig. 14. Steady state three phase grid voltage and currents in capacitive and inductive modes.

A. Operation of system in steady state

Fig. 8 shows the grid voltage V_s and grid current I_s in two different operating modes. In Fig. 8a, the current lags the voltage by 88˚ (inductive mode) while in Fig. 8b the current leads the voltage by 88˚ (capacitive mode). In both modes, the nominal reactive power is transferred and the Total Harmonic Distortion (THD) of current remains lower than 5%. Also in Fig. 9 the grid and the synthesized voltage by the inverter are illustrated. As previously mentioned and seen in Fig. 9, when the inverter injects reactive power to the grid, the fundamental harmonic of voltage is greater than the source voltage. On the other side, when the inverter absorbs reactive power, the

fundamental harmonic of voltage is lower than the source voltage.

Moreover, from Fig. 10 one can observe that the capacitors' voltages have been well regulated and the voltage ripple is less than 10% in both operating modes.

B. Operation of system in dynamic state

In dynamic states, the STATCOM should be able to generate both inductive and capacitive reactive power commands quickly, while the dc-link voltages remain constant.

In this paper, a stepwise reactive power change from full inductive mode to full capacitive mode is generated at t=15 s to verify the dynamic behavior of system. The obtained dynamic response is shown in Fig. 11. From Fig. 11, it is seen that the transient time does not take more than 40ms while the low frequency switching technique is employed.

Fig. 12 depicts the harmonic spectrum of inverter output voltage. It can be seen that the 5^{th} and 7^{th} harmonics have been almost eliminated (less than 1%), which confirms the satisfactory implementation of SHE method.

VI. EXPERIMENTAL RESULTS

To validate the proposed control and modulation method, a scaled down laboratory prototype has been implemented and is shown in Fig. 13. Since a three-phase two-cell inverter is used, all triplen harmonics are eliminated automatically in the line- to-line voltages. A floating point DSP processor (TMS320F28335) is used to implement the control and modulation approach. The experimental system parameters of CHB based STATCOM are listed in Table III. Similar to simulation study, the experimental results are investigated in steady state and dynamic condition. Fig. 14 shows the steady state behavior of three-phase system in capacitive and inductive modes. Also Fig. 15 illustrates the corresponding output waveforms in two operating modes.

Finally, Fig. 16 depicted the dynamic behavior of proposed approach in practice. In this test, the STATCOM is operated in inductive mode at first and at t_0 the operating mode is changed to capacitive mode in a stepwise manner. This figure also shows the voltage of dc-link capacitors in phase A under dynamic condition. As it can be seen, the voltages of capacitors remain constant and the grid current follows the command.

VII. CONCLUSION

This paper has presented a novel modulation method for asymmetric CHB inverters which employ low frequency switching method. In the PWM techniques, the efficiency of converter reduces due to high switching losses; but in this paper, the switching loss is kept as minimum as possible. By using asymmetric voltages for dc-links, the maximum number of voltage levels is synthesized at the output. This approach gives a better waveform in output of inverter, so the quality of power system will be enhanced. At the end, the simulation and experimental results confirmed the validity of proposed method in both steady state and dynamic conditions.

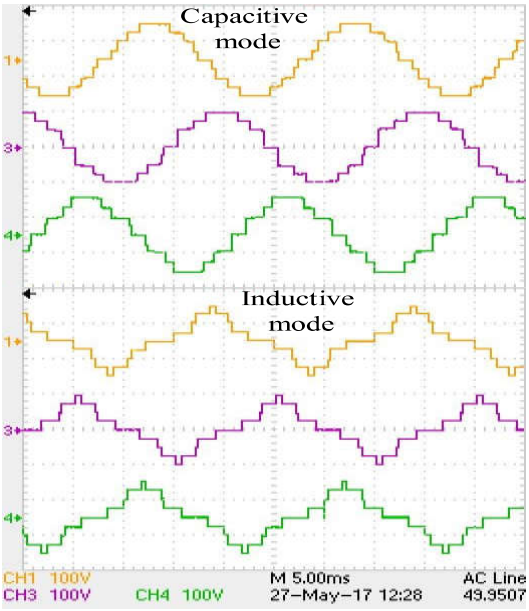

Fig. 15. Output waveform in capacitive and inductive modes.

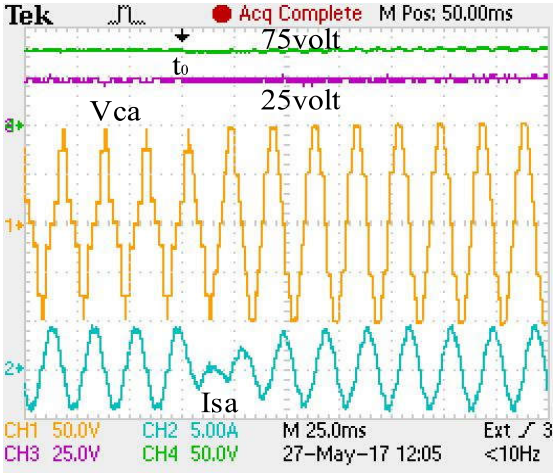

Fig. 16. Capacitor voltages, inverter voltage and grid current in dynamic state.

REFERENCES

[1] J. Rodriguez, J.-S. Lai, and F. Z. Peng, "Multilevel inverters: A survey of topologies, controls, and applications," *IEEE Trans. Ind. Electron.*, vol. 49, no. 4, pp. 724–738E, Aug. 2002.

[2] Y. Chen, B. Mwinyiwiwa, Z.Wolanski, and B.-T. Ooi, "Unified power flow controller (UPFC) based on chopper stabilized diode-clamped multilevel converters," *IEEE Trans. Power Electron.*, vol. 15, no. 2, pp. 258–267, Mar. 2000.

[3] Z. Ye *et al.*, "A Novel DC-Power Control Method for Cascaded H-Bridge Multilevel Inverter," in *IEEE Transactions on Industrial Electronics*, vol. 64, no. 9, pp. 6874-6884, Sept. 2017

[4] G. Farivar, B. Hredzak and V. G. Agelidis, "Reduced-Capacitance Thin-Film H-Bridge Multilevel STATCOM Control Utilizing an Analytic Filtering Scheme," in *IEEE Trans. Ind. Electron*, vol. 62, no. 10, pp. 6457-6468, Oct. 2015.

[5] C. D. Townsend, T. J. Summers and R. E. Betz, "Impact of Practical Issues on the Harmonic Performance of Phase-Shifted Modulation Strategies for a Cascaded H-Bridge StatCom," in *IEEE Trans. Ind. Electron*, vol. 61, no. 6, pp. 2655-2664, June 2014.

[6] C. K. Lee, J. S. K. Leung, S. Y. R. Hui, and H. S.-H. Chung, "Circuit level comparison of STATCOM technologies," *IEEE Trans. Power Del.*, vol. 18, no. 3, pp. 1084–1092, Jul. 2003.

[7] G. Farivar, C. D. Townsend, B. Hredzak, J. Pou and V. G. Agelidis, "Passive Reactor Compensated Cascaded H-Bridge Multilevel LC-

StatCom," in *IEEE Transactions on Power Electronics*, vol. 32, no. 11, pp. 8338-8348, Nov. 2017.

[8] Y. Zhang, X. Wu, X. Yuan, Y. Wang and P. Dai, "Fast Model Predictive Control for Multilevel Cascaded H-Bridge STATCOM With Polynomial Computation Time," in *IEEE Transactions on Industrial Electronics*, vol. 63, no. 8, pp. 5231-5243, Aug. 2016.

[9] S. Du, J. Liu, J. Lin and Y. He, "A Novel DC Voltage Control Method for STATCOM Based on Hybrid Multilevel H-Bridge Converter," in *IEEE Transactions on Power Electronics*, vol. 28, no. 1, pp. 101-111, Jan. 2013.

[10] Z. Zheng, K. Wang, L. Xu and Y. Li, "A Hybrid Cascaded Multilevel Converter for Battery Energy Management Applied in Electric Vehicles," in *IEEE Transactions on Power Electronics*, vol. 29, no. 7, pp. 3537-3546, July 2014.

[11] S. Mekhilef and M. N. Abdul Kadir, "Novel Vector Control Method for Three-Stage Hybrid Cascaded Multilevel Inverter," in *IEEE Transactions on Industrial Electronics*, vol. 58, no. 4, pp. 1339-1349, April 2011.

[12] Z. Liu, B. Liu, S. Duan and Y. Kang, "A Novel DC Capacitor Voltage Balance Control Method for Cascade Multilevel STATCOM," in *IEEE Transactions on Power Electronics*, vol. 27, no. 1, pp. 14-27, Jan. 2012.

[13] Y. Li and B. Wu, "A Novel DC Voltage Detection Technique in the CHB Inverter-Based STATCOM," in *IEEE Transactions on Power Delivery*, vol. 23, no. 3, pp. 1613-1619, July 2008.

[14] G. Farivar, B. Hredzak and V. G. Agelidis, "Decoupled Control System for Cascaded H-Bridge Multilevel Converter Based STATCOM," in *IEEE Transactions on Industrial Electronics*, vol. 63, no. 1, pp. 322-331, Jan. 2016.

[15] J. A. Barrena, L. Marroyo, M. Á. Rodriguez Vidal and J. R. Torrealday Apraiz, "Individual Voltage Balancing Strategy for PWM Cascaded H-Bridge Converter-Based STATCOM," in *IEEE Transactions on Industrial Electronics*, vol. 55, no. 1, pp. 21-29, Jan. 2008.

[16] J. I. Y. Ota, Y. Shibano and H. Akagi, "A Phase-Shifted PWM D-STATCOM Using a Modular Multilevel Cascade Converter (SSBC)—Part II: Zero-Voltage-Ride-Through Capability," in *IEEE Transactions on Industry Applications*, vol. 51, no. 1, pp. 289-296, Jan.-Feb. 2015.

[17] Y. Neyshabouri, H. Iman-Eini and M. Miranbeigi, "State feedback control strategy and voltage balancing scheme for a transformer-less STATic synchronous COMpensator based on cascaded H-bridge converter," *IET Power Electron*., vol. 8, no. 6, pp. 906-917, Jun. 2015.

[18] Fang Zheng Peng, J. W. McKeever and D. J. Adams, "A power line conditioner using cascade multilevel inverters for distribution systems," in *IEEE Transactions on Industry Applications*, vol. 34, no. 6, pp. 1293-1298, Nov/Dec 1998.

[19] H. Iman-Eini, J. L. Schanen, S. Farhangi and J. Roudet, "A Modular Strategy for Control and Voltage Balancing of Cascaded H-Bridge Rectifiers," in *IEEE Transactions on Power Electronics*, vol. 23, no. 5, pp. 2428-2442, Sept. 2008.

[20] M. Moosavi, G. Farivar, H. Iman-Eini and S. M. Shekarabi, "A voltage balancing strategy with extended operating region for cascaded H-bridge converters," in *IEEE Transactions on Power Electronics*, vol. 29, no. 9, pp. 5044-5053, Sept. 2014.

[21] K. Sano and M. Takasaki, "A Transformerless D-STATCOM Based on a Multivoltage Cascade Converter Requiring No DC Sources," in *IEEE Transactions on Power Electronics*, vol. 27, no. 6, pp. 2783-2795, June 2012.

[22] L. K. Haw, M. S. A. Dahidah and H. A. F. Almurib, "SHE–PWM Cascaded Multilevel Inverter With Adjustable DC Voltage Levels Control for STATCOM Applications," in *IEEE Transactions on Power Electronics*, vol. 29, no. 12, pp. 6433-6444, Dec. 2014.

[23] R. Lizana, M. A. Perez, D. Arancibia, J. R. Espinoza and J. Rodriguez, "Decoupled Current Model and Control of Modular Multilevel Converters," in *IEEE Transactions on Industrial Electronics*, vol. 62, no. 9, pp. 5382-5392, Sept. 2015.

[24] T. A. Lipo and M. D. Manjrekar, "Hybrid topology for multilevel power conversion," U.S. Patent 6 005 788, Dec. 21, 1999.

[25] H. Taghizadeh and M. Tarafdar Hagh, "Harmonic Elimination of Cascade Multilevel Inverters with Nonequal DC Sources Using Particle Swarm Optimization," in *IEEE Trans. Ind. Electron*, vol. 57, no. 11, pp. 3678-3684, Nov. 2010.

[26] A. Cetin and M. Ermis, "VSC-Based D-STATCOM With Selective Harmonic Elimination," in *IEEE Transactions on Industry Applications*, vol. 45, no. 3, pp. 1000-1015, May-june 2009.

[27] Marzoughi, A.; Neyshabouri, Y.; Imaneini, H., "Control scheme for cascaded H-bridge converter-based distribution network static compensator," Power Electronics, IET , vol.7, no.11, pp.2837,2845, 11 2014

Rahman Sajadi received the B.Sc. degree in electrical engineering from the Buali-Sina University, Hamedan, Iran, in 2014, and the M.Sc. degree in electrical engineering from the University of Tehran, Tehran, Iran, in 2016. His research interests include design, modeling and control of power converters, multilevel converters, and renewable energy systems.

Hossein Iman-Eini (M' 10-SM' 17) received the B.S. and M.S. degrees from the University of Tehran, Iran in 2001 and 2003, respectively, and the Ph.D. degree jointly from the University of Tehran and the Grenoble INP, Grenoble, France in 2009, all in electrical engineering. He is currently an Associate Professor in the School of ECE, University of Tehran. His current research interests include the modeling and control of power converters and renewable energy systems.

Mohammad Kazem Bakhshizadeh (S'16) received the B.S. and M.S. degrees in electrical engineering from the Amirkabir University of Technology, Tehran, Iran, in 2008 and 2011, respectively. He is currently an Industrial Ph.D. student with Aalborg University, Aalborg, Denmark. His current research interests include power quality, modeling and control of power converters, and grid converters for renewable energy systems.

Yousef Neyshabouri received the B.Sc. and M.Sc. degrees in electrical engineering from the University of Tehran, Tehran, Iran, in 2011 and 2013, respectively. He is currently working toward the Ph.D. degree at the University of Tehran. His research interests include power converters and their application in FACTs and renewable energy systems.

Shahrokh Farhangi (M' 90) obtained the B.Sc., M.Sc. and Ph.D. degrees in electrical engineering from University of Tehran, Iran, with honors. He is currently professor of School of Electrical and Computer Engineering, University of Tehran. His research interests include design and modeling of Power Electronic Converters, Drives, Photovoltaics and Renewable Energy Systems.